6. M.-F. Lei and H. Wang, An analysis of miniaturized dual-mode bandpass filter structure using shunt-capacitance perturbation, IEEE Trans Microwave Theory Tech 53 (2005), 861–867.
7. J.-T. Kuo and C.-Y. Tsai, Periodic stepped-impedance ring resonator (PSIRR) bandpass filter with a miniaturized area and desirable upper stopband characteristics, IEEE Trans Microwave Theory Tech 54 (2006), 1107–1112.
8. R.-B. Wu and S. Amari, New triangular microstrip loop resonators for bandpass dual-mode filter application, MTT-S Int Microwave Symp Dig, Long Beach, CA, 2005, 941–944.
9. R.-J. Mao and X.-H. Tang, Novel dual-mode bandpass filters using hexagonal loop resonators, IEEE Trans Microwave Theory Tech 54 (2006), 3526–3533.
10. R.-J. Mao, X.-H. Tang, and F. Xiao, Miniaturized dual-mode ring bandpass filters with patterned ground plane, IEEE Trans Microwave Theory Tech 55 (2007), 1539–1547.
11. Y.-C. Chiou, J.-T. Kuo, and J.-S. Wu, Miniaturized dual-mode ring resonator bandpass filter with microstrip-to-CPW broadside-coupled structure, IEEE Microwave Wireless Compon Lett 18 (2008), 97–99.
12. S. Otto, A. Rennings, C. Caloz, and P. Waldow, Dual mode zeroth order ring resonator with tuning capability and selective mode excitation, Eur Microwave Conf Dig 1 (2005), 4–6.
13. C.A. Allen, K.M.K.H. Leong, and T. Itoh, Dual-mode composite-right/left-handed transmission line ring resonator, Electron Lett 42 (2006), 96–97.
14. W. Tong and Z. Hu, Left-handed L-band notch bandstop filter with significantly reduced size, IET Microwave Antennas Propag 1 (2007), 45–49.
15. J.D. Baena, J. Bonache, F. Martin, R. Marques, F. Falcone, T. Lopetegi, M.A.G. Laso, J. Garcia, I. Gil, M.F. Portillo, and M. Sorolla, Equivalent-circuit models for split-ring resonators and complementary split-ring resonators coupled to planar transmission lines, IEEE Trans Microwave Theory Tech 53 (2005), 1451–1461.
16. J.-X. Niu and X.-L. Zhou, A novel miniaturized hybrid ring using complementary split ring resonators, Microwave Opt Technol Lett 50 (2008), 632–635.
17. G.-B. Xiao and K. Yashiro, On the design of a dual-mode ring resonator formed by nonuniform transmission lines, Int J Electron 89 (2002), 337–345.
18. A.C. Kundu and I. Awai, Control of attenuation pole frequency of a dual-mode microstrip ring resonator bandpass filter, IEEE Trans Microwave Theory Tech 49 (2000), 1113–1117.

FREQUENCY-INDEPENDENT PERFORMANCE OF ELLIPTIC PROFILE TEM HORNS

Jag Malherbe
Department of Electrical, Electronic and Computer Engineering, University of Pretoria, Pretoria 0002, South Africa; Corresponding author: jagm@up.ac.za

Received 9 July 2008

ABSTRACT: *The TEM horn with elliptic E-plane profile has been shown to give extremely wide bandwidth performance as far as VSWR and gain is concerned. In this article, the variation in radiation pattern versus frequency is explored, and it is shown that, dependant on choice, E-plane or H-plane radiation patterns that are virtually independent of frequency can be obtained.* © 2009 Wiley Periodicals, Inc. Microwave Opt Technol Lett 51: 607–612, 2009; Published online in Wiley InterScience (www.interscience.wiley.com). DOI 10.1002/mop.24109

Key words: *TEM horn; elliptic profile; frequency-independent properties*

1. INTRODUCTION

The so-called TEM horn has proven to be extremely popular for the realization of very wide bandwidth performance, where gain and input VSWR are concerned. Various approaches to realizing the desired wide bandwidths are employed, making use variously of impedance and dimensional tapers [1–6]. In all cases, the emphasis is on obtaining wideband performance, mostly for impedance. The analytical description of the TEM horn is extremely limited, with the exception of [7], where the characteristic impedance of the radial lines that constitute the TEM horns on a point-by-point basis is derived. Thus, to date approaches to design are limited to the realization of the best impedance match, making use of the information of [7], in combination with the various tapers. Little or no effort is made to present information as to the effect of dimensions on parameters such as gain or radiation pattern as a function of frequency.

Recently, the application of an elliptic function to describe the plate separation was introduced [4–6], and it was shown that extremely wideband performance could be achieved. However, the radiation pattern properties were not considered per se. It was shown in [6] that very good agreement could be achieved between measured values on a physically constructed horn, and numerical analysis by means of the commercial software FEKO© [8] for a number of variables.

In this article, the validity of the numerical analysis employed in the calculation of horn properties is re-established by extensive comparison of additional measured and calculated

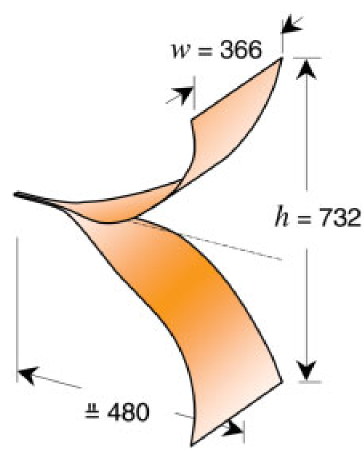

Figure 1 Horn dimensions (mm) [6]. [Color figure can be viewed in the online issue, which is available at www.interscience.wiley.com]

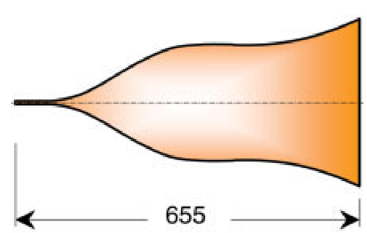

Figure 2 Unfolded horn plate (mm). [Color figure can be viewed in the online issue, which is available at www.interscience.wiley.com]

values of radiation pattern for the horn described in [6]. Once it is confirmed that the numerical model properly approximates the physical structure, the numerical analysis is used to evaluate the properties of a series of horns, designed by the procedure described in [6], through a systematic variation of dimensions. From this information, the structure of TEM horns that displays virtually frequency-independent radiation patterns in some planes is identified.

2. HORN ANALYSIS: CALIBRATION

To establish the validity of the numerical analysis, radiation patterns for both *E*- and *H*-planes were measured on the pro-

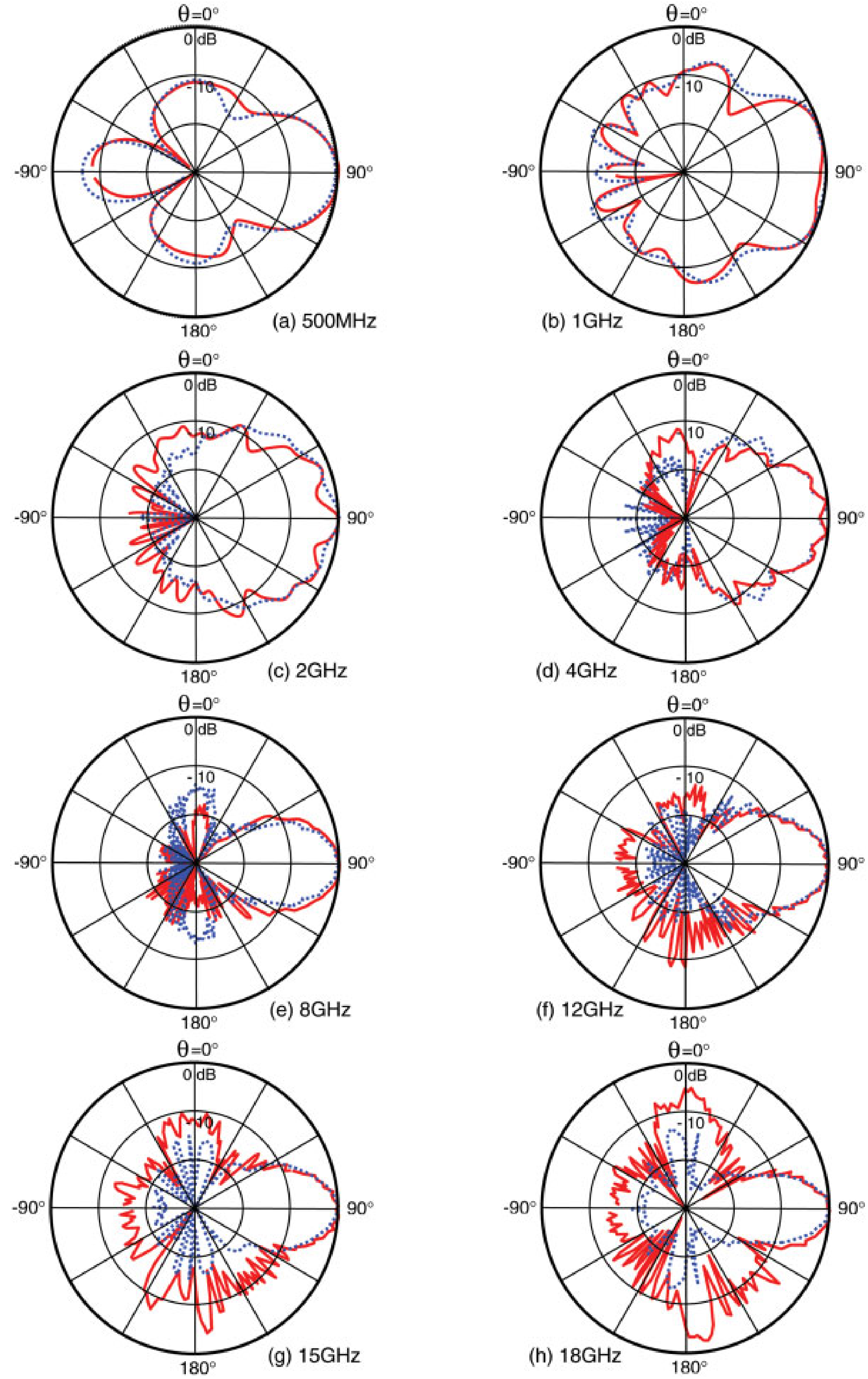

Figure 3 Comparison of measured and calculated *E*-plane radiation patterns over the band 0.5–18 GHz for the extreme bandwidth horn. [Color figure can be viewed in the online issue, which is available at www.interscience.wiley.com]

totype, as well as calculated at 0.5, 1, 2, 4, 8, 12, 15, and 18 GHz. Previously, the horn was analyzed only at 05, 4, and 12 GHz [6].

The horn described in [6] is electrically very large, with overall dimensions of horn length of 480 mm, a width of 366 mm, and a height of 732 mm, as shown in Figure 1. At 18 GHz, this corresponds to a structure of 29 × 22 × 44 wavelengths. When folded flat, the two horn plates each measures 655 mm × 367 mm, as shown in Figure 2 (40 × 22 wavelengths). In the numerical model, the horn plates were divided into triangles of

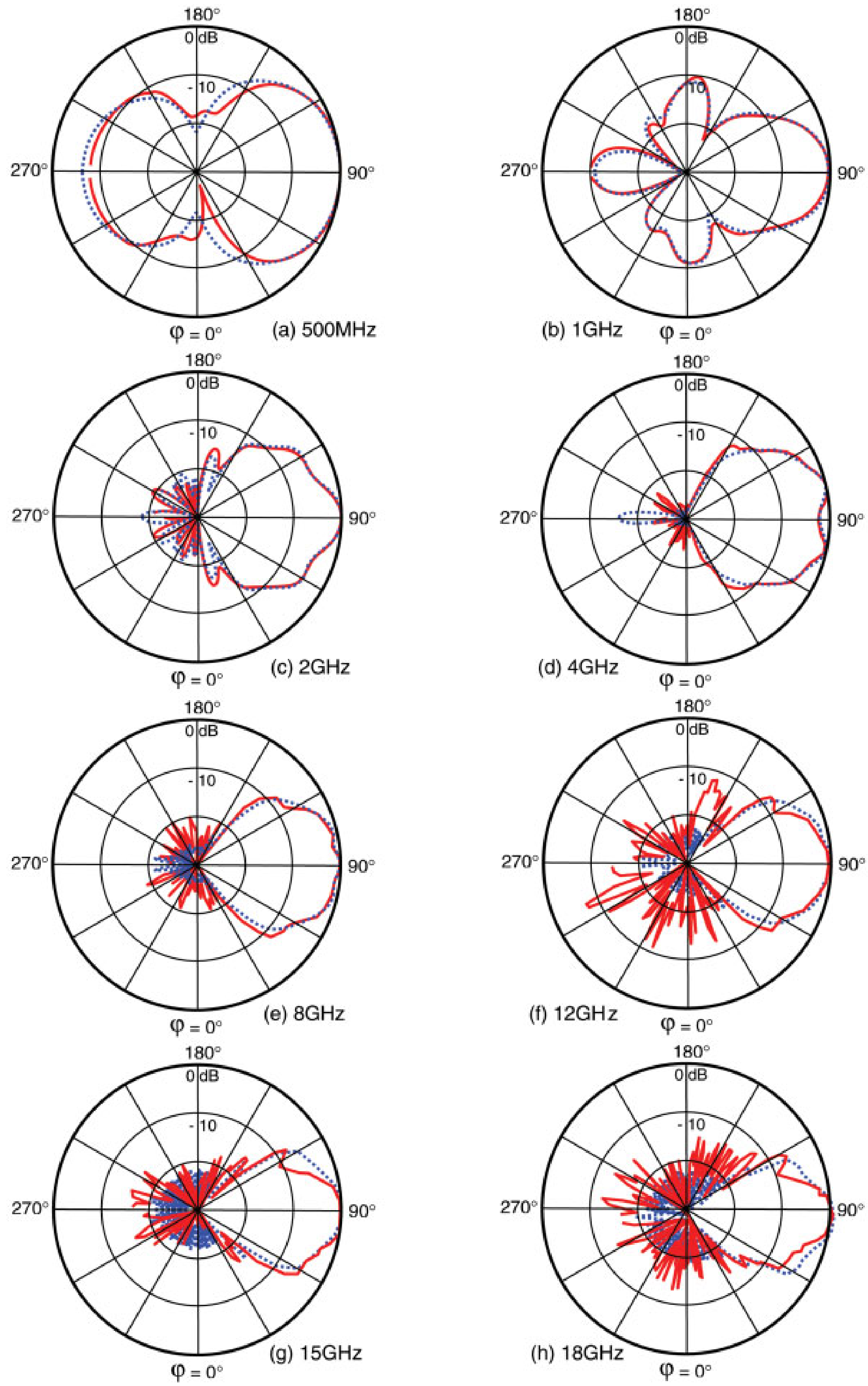

Figure 4 Comparison of measured and calculated *H*-plane radiation patterns over the band 0.5–18 GHz for the extreme bandwidth horn. [Color figure can be viewed in the online issue, which is available at www.interscience.wiley.com]

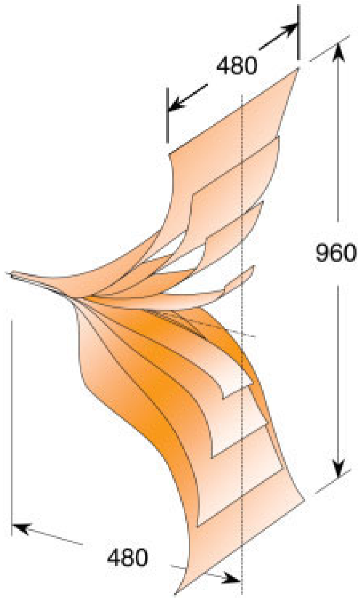

Figure 5 Comparison of horns 240–480, 480–480, 732–480, 960–480. [Color figure can be viewed in the online issue, which is available at www.interscience.wiley.com]

maximum size λ/8 on any side at the highest frequency of analysis. Figures 3(a)–3(h) show the *E*-plane radiation patterns comparing measured and calculated values, whereas the corresponding patterns are given for the *H*-plane in Figures 4(a)–4(h).

The correspondence between the measured and calculated values is excellent for both polarizations and across the entire frequency range, at least for the main beams and down to a level of −10 dB. At frequencies above about 15 GHz, some of the minor sidelobes lie outside of this level.

Because of this extent of agreement, the numerical analysis can now be used with confidence to predict the properties of a series of horns of varying dimensions that constitute a parametric study of the elliptic profile TEM horn.

3. PARAMETRIC EVALUATION OF HORN PROPERTIES: CALCULATION

The parametric evaluation of the elliptic profile horn was performed on a series of four horns, all with the same length of 480 mm, but with heights of 240, 480, 732, and 960 mm, respectively, as shown in Figure 5; the nominal horn dimensions in mm are given in Table 1. Note that although the horn length is fixed, both height and width change simultaneously, in order that the impedance determined by the Hecken taper described in [6] is realized. Longer or shorter lengths of horn will give the same performance for the same aspect ratio as the principle of frequency scaling can be applied. The horn 732–480 serves as reference.

E- and *H*-plane patterns were calculated for frequencies at 1 GHz intervals between 1 and 18 GHz, and the radiation patterns from 3 to 18 GHz plotted on the same axes as shown in Figure 6 for both the *E*- and *H*-planes (this constitutes a total of 16 radiation patterns on each polar pattern).

The calculated gain and VSWR performance for the four horns is shown in Figures 7 and 8, respectively.

4. EVALUATION

The radiation properties of elliptic profile horns are discussed in [5], where it is shown that the lowest operating frequency of the horn corresponds to a total horn length of one-half wavelength (measured along the surface of the horn). This is termed the first dipole mode, and more dipole modes occur as the frequency is increased, until the horn radiates sufficient energy in the aperture direction so that the structure functions as a horn rather than a dipole.

For all of the horns analyzed, the radiation patterns showed that at frequencies below 3 GHz, the dipole effect was still very strong, as evidenced by periodic variations in gain and impedance. Also, the radiation patterns strongly exhibit dipole characteristics, as can be seen in Figures 3(a) and 3(b) and 4(a) and 4(b). Consequently, radiation patterns below 3 GHz were not included in the polar patterns of Figure 6.

As the horn height is increased, the various horns retain nominally the same main lobe width in the *E*-plane at about 20°. The small horn (240–480) has the smallest spread of *E*-plane radiation pattern with frequency, being almost frequency-independent over the entire 3–18 GHz band [Fig. 6(a)]. As the horn aspect ratio increases, the *E*-plane spread increases.

In the *H*-plane, however, the small horn has a radiation pattern that varies substantially with frequency. As the aspect ratio is increased, the *H*-plane radiation pattern spread decreases, until the smallest spread is observed for an aspect ratio of ~1 [Fig. 6(b)]. Beyond that, the spread in *H*-plane radiation pattern increases again with increasing aspect ratio. At the same time, there is a substantial increase in beamwidth. The increase in beamwidth is accompanied by a decrease in gain. For all cases, the gain remains fairly flat with frequency.

All the horns display nominally the same VSWR performance, except at the lower frequencies, where the larger horns obviously have a lower dipole mode. This is to be expected as all the horns were designed with the same Hecken impedance taper. The VSWR remains below 2 from 1 GHz upward, and for all the horns rises above 2 at around 12 GHz, remaining below 3–18 GHz. This is not perturbing, as impedance analysis showed that the reactive part of the input impedance increases uniformly with frequency, whereas the real part is constantly too high. It would therefore be easy to correct the high-frequency performance, and will cause little degradation at low frequencies.

5. CONCLUSIONS

This parametric analysis of the elliptical profile TEM horn design has shown that such horns can be designed to give a predetermined performance. The overall length of the horn is determined by the lowest operating frequency, whereas the type of *H*-plane radiation

TABLE 1 Horn Dimensions

Horn Designation	Length l (mm)	Height h (mm)	Width w (mm)	h/l
240–480	480	240	120	0.50
480–480	480	480	240	1.00
732–480	480	732	366	1.525
960–480	480	960	480	2.00

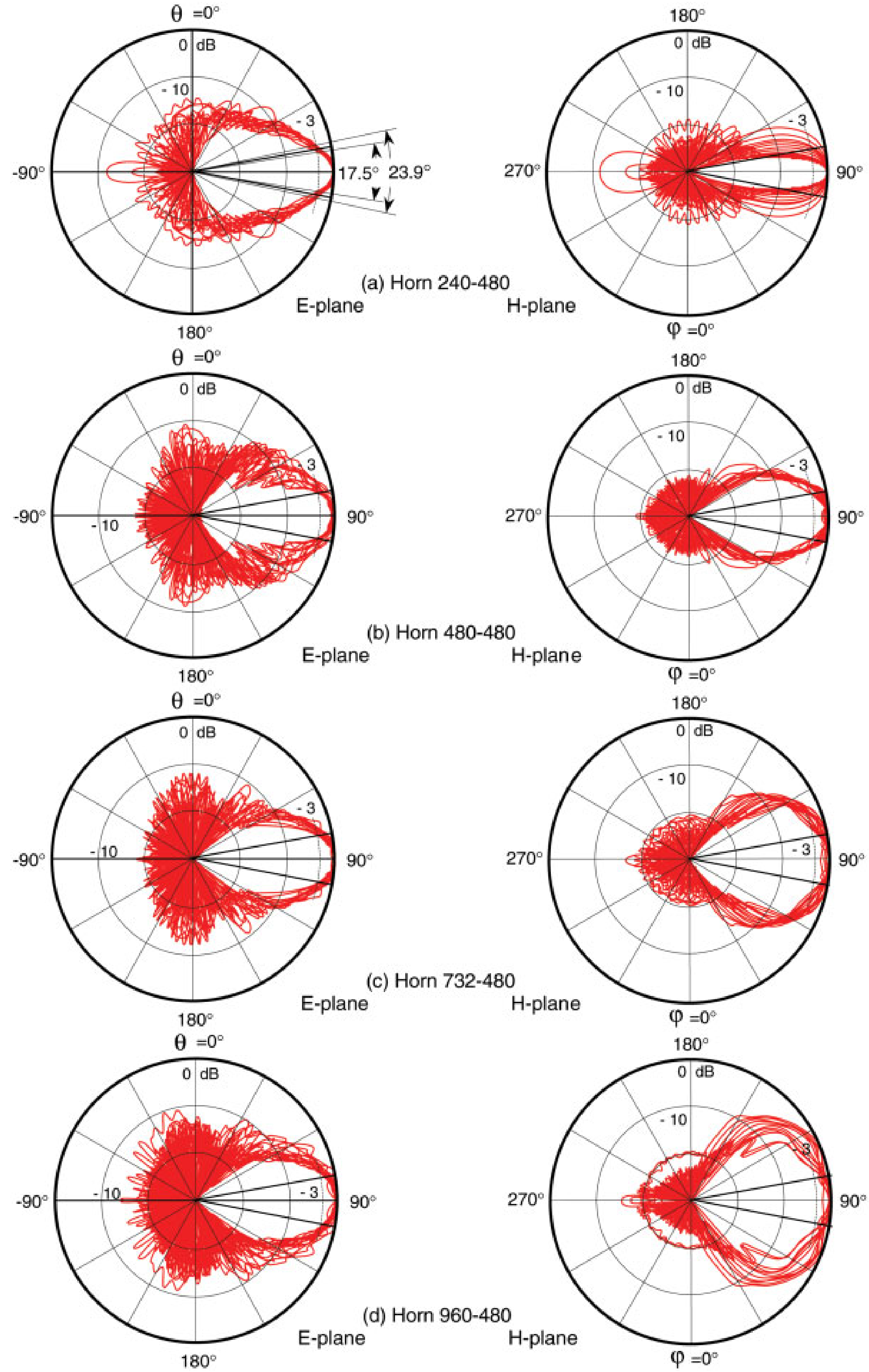

Figure 6 Grouped radiation patterns at 1 GHz intervals for various horns. *E*- and *H*-planes. [Color figure can be viewed in the online issue, which is available at www.interscience.wiley.com]

pattern or gain will determine the horn aspect ratio. The *E*-plane radiation pattern is fixed.

A horn aspect ratio of approximately unity gives *E*- and *H*-plane radiation patterns that are not only approximately equal in size but also to a very large extent frequency-independent.

ACKNOWLEDGMENTS

The author wishes to express his sincere appreciation for the support from the FEKO staff, Mel van Rooyen, Danie le Roux, and Robert Kellerman, who assisted in making calculationsand provided extensive support in developing the numerical models.

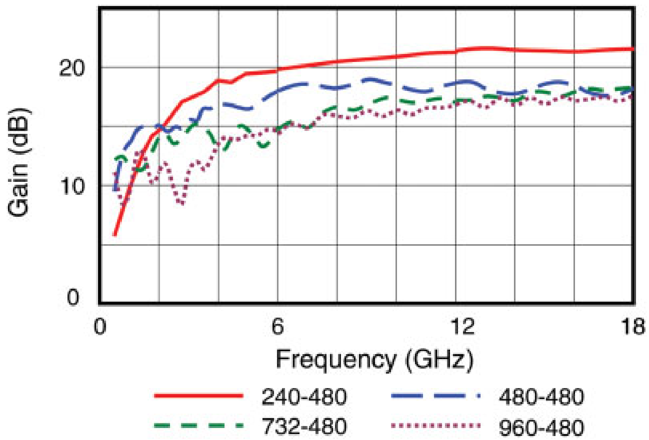

Figure 7 Calculated gain vs. frequency. [Color figure can be viewed in the online issue, which is available at www.interscience.wiley.com]

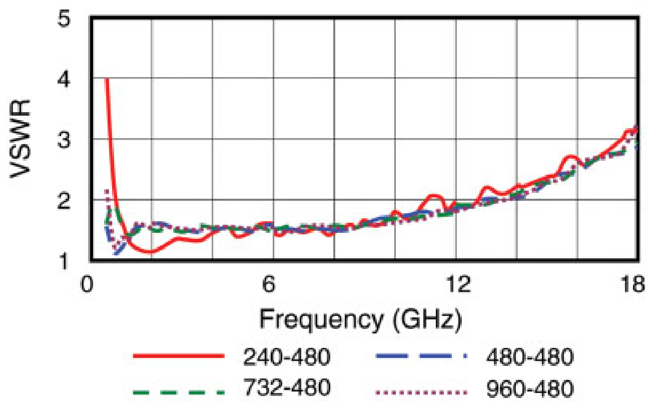

Figure 8 Calculated VSWR vs. frequency. [Color figure can be viewed in the online issue, which is available at www.interscience.wiley.com]

REFERENCES

1. H. Choi and S. Lee, Design of an exponentially-tapered TEM horn antenna for the wide broadband communication, Microwave Opt Technol Lett 40 (2004), 531–534.
2. Y. Huang, M. Nakhkash, and J.T. Zhang, A dielectric material loaded TEM horn antenna, ICAP 2003, 12th Intl Conf Ant Prop, ICAP 2003, (Conf. Publ. No. 491) 2 (2003), 489–492.
3. A.S. Turk, Ultra-wideband TEM horn design for ground penetrating impulse radar systems, Microwave Opt Technol Lett 41 (2004), 333–336.
4. J.A.G. Malherbe and N.S. Barnes, TEM horn antenna with an elliptic profile, Microwave Opt Technol Lett 49 (2007), 1548–1551.
5. J.A.G. Malherbe, Design of ultra wideband TEM horns, Asia Pacific Microwave Conference, APMC 2007, Bangkok, Thailand, 2007.
6. J.A.G. Malherbe, Extreme performance TEM horn, Microwave Opt Technol Lett, in press; Available at: http://www3.interscience.wiley.com/cgi-bin/fulltext/119427859/PDFSTART.
7. K.L. Shlager, G.S. Smith, and J.G. Maloney, Accurate analysis of TEM horn antennas for pulse radiation, IEEE Trans Electromagn C, 38 (1996), 414–423.
8. FEKO©; EM Software & Systems-S.A. (Pty) Ltd. Available at: http://www.feko.info/index.html.

FLAT-PLATE PENTAGONAL MONOPOLE ANTENNA FOR LAPTOP WIRELESS COMMUNICATION AND MOBILE TV RECEPTION

Lev Pazin and Yehuda Leviatan
Department of Electrical Engineering, Technion-Israel Institute of Technology, Haifa 32000, Israel; Corresponding author: leviathan@ee.technion.ac.il

Received 9 July 2008

ABSTRACT: *An improved novel printed wideband flat-plate monopole antenna is presented. The proposed antenna consists of a pentagonal monopole embedded in a corner notch in the antenna ground plane part. Simulated and measured results of the input return loss for the proposed antenna are in good agreement. The antenna has been shown to operate satisfactorily in the 0.47–6 GHz frequency range, and is therefore very suitable for use as antenna for laptop applications including Wi-Fi, WiMAX, and mobile TV reception.* © 2009 Wiley Periodicals, Inc. Microwave Opt Technol Lett 51: 612–615, 2009; Published online in Wiley InterScience (www.interscience.wiley.com). DOI 10.1002/mop.24133

Key words: *mobile antenna; wideband antenna; pentagonal monopole*

1. INTRODUCTION

Several antennas for TV reception that can be integrated into laptop computers have recently been proposed [1–5]. All these antennas are of a monopole-type, where the monopole either extends beyond the edge of the antenna ground plane part [1, 2] or is embedded in a notch in the antenna ground plane part [3–5]. Although the antennas proposed in [1–4] are exclusively for TV reception, the slotted triangular flat-plate printed monopole antenna suggested in [5] is perhaps the first multiband antenna which is suitable not only for DVB-H TV reception in the 0.47–0.87 GHz frequency range but also for Wi-Fi (2.4–2.5 GHz and 5.15–5.875 GHz) and WiMAX (2.3–2.4 GHz, 2.5–2.7 GHZ, and 3.4–3.6 GHz) applications. In this article, we propose a flat-plate printed monopole antenna that is similar to the one suggested in [5]. However, unlike the antenna in [5], which is multiband and yields a somewhat low average gain of −4.55 dB at 5.5 GHz, the new antenna covers the entire 0.47–6 GHz frequency range (bandwidth of approximately 13:1) and yields a much higher average gain. The proposed antenna consists of a pentagonal base-fed monopole of unequal sides embedded in a corner notch in the antenna ground plane part. The monopole part should extend beyond the edge of the laptop lid during the wireless operation of the laptop. Toward this end, the monopole part can be deployed using a flip-up and -down mechanism [1]. Alternatively, the monopole part can be pulled out from the screen lid as suggested in [2]. The new antenna was simulated using the commercial CST Microwave Studio software. The antenna has also been fabricated and its return loss was measured using an Agilent N5230A network analyzer. The results of the simulations and measurements, demonstrating the desired operation of the antenna in the 0.47–6 GHz frequency range, were found to be in good agreement.

2. ANTENNA DESIGN

The geometry of the proposed antenna is shown in Figure 1. The size of the antenna is 240 mm × 175 mm. The height of the pentagonal monopole is 120 mm and the width of its base is 50 mm. Both the monopole and the ground plane parts are printed on one side of a hard no-ground RT5880 substrate with relative